Critical behavior of charmonia across the phase transition: A QCD sum rule approach

Kenji Morita* and Su Houng Lee†
Institute of Physics and Applied Physics, Yonsei University, Seoul 120-749, Korea
(Received 26 November 2007; revised manuscript received 30 April 2008; published 10 June 2008)

We investigate the medium-induced change of mass and width of J/ψ and η_c across the phase transition in hot gluonic matter using QCD sum rules. In the QCD sum rule approach, the medium effect on heavy quarkonia is induced by the change of both scalar and twist-2 gluon condensates, whose temperature dependencies are extracted from the lattice calculations of energy density and pressure. Although the stability of the operator product expansion side seems to break down at $T > 1.06T_c$ for the vector channel and $T > 1.04T_c$ for the pseudoscalar channel, we find a sudden change of the spectral property across the critical temperature T_c, which originates from an equally rapid change of the scalar gluon condensate characterized by $\varepsilon - 3p$. By parametrizing the ground state of the spectral density by the Breit-Wigner form, we find that for both J/ψ and η_c, the masses suddenly decrease maximally by a few hundreds of MeV and the widths broaden to ~100 MeV slightly above T_c. The implications for recent and future heavy-ion experiments are discussed. We also carry out a similar analysis for charmonia in nuclear matter, which could serve as a testing ground for observing the precursor phenomena of the QCD phase transition. We finally discuss the possibility of observing the mass shift at nuclear matter at the FAIR project at GSI.

DOI: 10.1103/PhysRevC.77.064904 PACS number(s): 12.38.Mh, 11.55.Hx, 14.40.Gx, 24.85.+p

I. INTRODUCTION

The in-medium change of spectral properties of heavy quarkonia is one of the interesting problems in recent hadron physics. First, the recent relativistic heavy-ion collision experiment at the Relativistic Heavy Ion Collider (RHIC) has revealed the exciting nature of QCD matter through a number of observations [1–5]. However, there are many open questions involving both experimental facts and our theoretical understanding of QCD matter. Hence, it is important to establish appropriate experimental observables that reflect the consequences of a deeper theoretical understanding of the matter. Heavy quarkonia have been regarded as one of the most suitable diagnostic tools in this respect, since the suppression of J/ψ yields would reflect the Debye screening phenomenon caused by the deconfinement phenomenon in the quark-gluon plasma (QGP), as was originally argued by Matsui and Satz [6]. Until now, quarkonium production, especially that of J/ψ, in relativistic heavy-ion collisions has been extensively studied both experimentally [7,8] and theoretically [9,10]. However, remarkable progress comes from recent lattice QCD calculations, which indicate that, contrary to the earlier expectation, the J/ψ will survive as a bound state even in the QGP up to $T \sim (1.6\text{–}2)T_c$ [11–13], which had been anticipated based on the nonperturbative nature of QGP [14]. Nowadays, the state of matter at this temperature region has been characterized as "strongly coupled" QGP (sQGP). Hence, there will be change of spectral properties even for a heavy-quark system that has to be considered in interpreting experimental observables.

Second, charmonium in a nuclear medium is also an interesting issue. In relativistic heavy-ion collisions, we need knowledge of the quarkonium-nucleon interaction to discriminate the suppression by QGP from the "cold nuclear matter effect" induced by such an interaction. Furthermore, multigluon exchange can lead to an attractive interaction between $c\bar{c}$ and a nucleon, which may result in a bound state of charmonium and light nuclei, as pointed out by Brodsky *et al.* [15]. It should also be noted that the planned Panda experiment at GSI-FAIR involves reaction of antiprotons with a nucleus target, which will yield charmonia in nuclear matter. It could serve as a testing ground for observing the precursor phenomenon of the QCD phase transition.

In this paper, we investigate the change of mass and width of J/ψ and η_c induced by strongly interacting hot gluonic matter and by the nuclear medium using QCD sum rule. The QCD sum rule provides a systematic procedure for studying hadrons from a viewpoint of the asymptotic freedom in QCD [16,17]. Since the QCD sum rule can take nonperturbative effects into account through the condensate terms, it is a suitable theoretical tool for the current study. Indeed, QGP at $T < 3T_c$ cannot be understood by using perturbation theory alone [18]. Furthermore, the sum rule is more promising for heavy-quark systems because we do not have to take the quark-antiquark condensate into account as we do for light-quark systems. In this respect, the sum rule has been applied to charmonium and bottonium. Shifman *et al.* established the framework in Refs. [16,17] and Reinders *et al.* extended it to the deep Euclidean region $Q^2 = -q^2 > 0$ [19] for the vacuum case. For in-medium quarkonia, one of us together with Furnstahl and Hatsuda has investigated the mass shift of J/ψ in hot hadronic matter [20], using a QCD sum rule approach, where the temperature effect was introduced to the perturbative Wilson coefficient through the scattering terms. A consistent formalism at lower density was developed by one of us [21] and independently by Hayashigaki [22] to study the mass shift of J/ψ in nuclear matter.

*morita@phya.yonsei.ac.kr
†suhoung@phya.yonsei.ac.kr

Along this direction, we investigated the mass shift and width broadening of J/ψ in hot gluonic plasma (GP) [23] just above the phase transition by consistently using the exact temperature dependencies of condensates from the lattice calculation. In the present paper, as a subsequent paper to Ref. [23], we present details of the analysis and further application to η_c and to spectral changes in nuclear matter.

In the next section, we will give an explanation of the QCD sum rule for heavy quarkonium in medium used in the present work. Sections III and IV describe the details of the numerical computations of the sum rule for hot gluonic matter and the nuclear medium, respectively. Section V is devoted to discussion and summary.

II. QCD SUM RULE FOR HEAVY QUARKONIUM

In this section, first we review the sum rule for heavy quarkonium in vacuum [19]. Then we introduce the extension to finite temperature and nuclear medium cases, in which the medium effect is eventually induced only by the expectation values of gluonic operators without any additional change in the operator product expansion (OPE).

A. Moment sum rule in vacuum

We start with the time-ordered current-current correlation function for the J channel,

$$\Pi^J(q) = i\int d^4x e^{iq\cdot x}\langle T[j^J(x)j^J(0)]\rangle, \tag{1}$$

where we consider the $J = P$ (pseudoscalar) and V (vector) currents of the heavy quark. Namely, $j^P = i\bar{c}\gamma_5 c$ and $j^V_\mu = \bar{c}\gamma_\mu c$ for charm. The expectation value $\langle\cdots\rangle$ is taken for the vacuum. If we go to the deep Euclidean region $Q^2 \equiv -q^2 \gg 0$, the product of the current can be expanded via the OPE [24]. If we denote $\tilde{\Pi}(q^2)$ such that $\Pi^{\mu\nu}(q) = (q^\mu q^\nu - q^2 g^{\mu\nu})\tilde{\Pi}(q^2)$ for the vector current, $\tilde{\Pi}(q^2)$ can be written as

$$\tilde{\Pi}^J(q^2) = \sum_n C_n^J \langle O_n\rangle, \tag{2}$$

where O_n are the operators of mass dimension n renormalized at scale μ^2 and C_n^J are the Wilson coefficients. By virtue of a much heavier quark mass than the confinement scale, heavy-quark operators, such as $m_c\bar{c}c$ for dimension four, are rewritten in terms of gluonic operator with a factor of $1/m_c$ via a heavy-quark expansion [16,25]. Hence, only gluonic operators contribute to the OPE for the heavy-quark currents.

The correlation function given by Eq. (2) is related to its imaginary part through the dispersion relation

$$\tilde{\Pi}^J(q^2) = \frac{1}{\pi}\int_{4m_c^2}^\infty \frac{\mathrm{Im}\,\tilde{\Pi}^J(s)}{s-q^2}ds, \tag{3}$$

where we ignore $+i\varepsilon$ in the denominator of the integrand since $q^2 = -Q^2 < 0$. Taking the nth derivative of Eqs. (2) and (3) as

$$M_n^J(Q^2) \equiv \frac{1}{n!}\left(\frac{d}{dq^2}\right)^n \tilde{\Pi}^J(q^2)\Big|_{q^2=-Q^2}, \tag{4}$$

we obtain the nth-order moments of

$$M_n^J(Q^2)_{\mathrm{OPE}} = A_n^J(\xi)\left[1 + a_n^J(\xi)\alpha_s + b_n^J(\xi)\phi_b\right] \tag{5}$$

for the OPE side and

$$M_n^J(Q^2)_{\mathrm{phen.}} = \frac{1}{\pi}\int_{4m_c^2}^\infty \frac{\mathrm{Im}\,\tilde{\Pi}^J(s)}{(s+Q^2)^{n+1}}ds \tag{6}$$

for the phenomenological (dispersion) side. Here, we have introduced a dimensionless scale variable $\xi = Q^2/4m_c^2$. In Eq. (5), $A_n^J(\xi)$, $a_n^J(\xi)$, and $b_n^J(\xi)$ are the Wilson coefficients that correspond to bare loop diagrams, perturbative radiative correction up to order α_s, and scalar gluon condensate, respectively. These coefficients were derived in Ref. [19] and we summarize them in the Appendix.

In evaluation of spectral properties, we take the ratio of the $(n-1)$th moment to the nth moment and equate the OPE side with the phenomenological side. Then we obtain the sum rule

$$\left.\frac{M_{n-1}^J}{M_n^J}\right|_{\mathrm{OPE}} = \left.\frac{M_{n-1}^J}{M_n^J}\right|_{\mathrm{phen.}}, \tag{7}$$

which relates the hadron properties (r.h.s.) with asymptotically free QCD (l.h.s.).

B. Moment sum rule for the hot gluonic medium

In this paper, we first consider the gluonic medium at finite temperature around T_c. Then, the expectation value in Eq. (1) is taken as $\langle\mathcal{O}\rangle = \mathrm{Tr}(e^{-\beta H}\mathcal{O})/\mathrm{Tr}(e^{-\beta H})$. Hereafter, we set both medium and $c\bar{c}$ at rest. We denote $q^\mu = (\omega, \boldsymbol{q})$ and take the $\boldsymbol{q} \to 0$ limit. In this case, the transverse and the longitudinal components of the correlation function for the vector channel are simply related with $\Pi_T = \omega^2\Pi_L$ and $\Pi_L = \Pi^\mu_\mu/(-3\omega^2)$. We denote the longitudinal component as $\tilde{\Pi}^J(\omega)$ for the vector channel.

At finite temperature, the *retarded* correlation function is related to the spectral function [26]. In the Euclidean region $\omega^2 < 0$, the retarded correlation function $\Pi^R(\omega)$ becomes $\Pi(\omega^2)$ and the dispersion relation is given by [20,27]

$$\tilde{\Pi}^J(\omega^2) = \int_{0^-}^\infty du^2 \frac{\rho(u)}{u^2-\omega^2}, \tag{8}$$

where $\rho(u)$ is the spectral function connecting with the imaginary part as

$$\rho(u) = \frac{1}{\pi}\tanh\left(\frac{u}{2T}\right)\mathrm{Im}\tilde{\Pi}^J(u^2). \tag{9}$$

Then Eq. (8) reduces to the vacuum case [Eq. (3)] when $\mathrm{Im}\tilde{\Pi}^J(u^2)$ has nonzero value only at $u \gg T$. Since we are interested in charmonia for which the mass is much larger than the temperature considered here, this condition seems to be appropriate one. However, there are formally two additional terms in the finite temperature spectral function [28]. One is the continuum part, which also exists in the vacuum case. Following the prescription in Ref. [19], we can suppress contribution from this part as described later because this part has finite values beyond some threshold. The other part arising from scattering of the current with quarks in medium is proportional to $\delta(u^2)$ and the contribution grows

with T in the hadronic medium [20]. However, since we are considering the *gluonic* medium in which there are no (anti)quarks that annihilate with the current, such a scattering term does not appear. Hence, we can use the same expression of the phenomenological side as in the vacuum case [Eq. (6)] for charmonia in the hot gluonic medium.

For the OPE side, there is an important change from the vacuum case to the medium one. Since we no longer have Lorentz invariance, nonscalar operators have nonvanishing values [27]. In the present case, the twist-2 gluon operator has a leading contribution and the nth-order moment of the OPE side [Eq. (5)] should be modified to

$$M_n^J(Q^2)_{\rm OPE} = A_n^J(\xi)\big[1 + a_n^J(\xi)\alpha_s + b_n^J(\xi)\phi_b + c_n^J(\xi)\phi_c\big], \tag{10}$$

where c_n and ϕ_c are the Wilson coefficients and the medium expectation value for the twist-2 operator. Since we are considering heavy-quark systems, only the condensate terms are temperature dependent as long as $T \ll m_c, |Q|$ [20,27]. Hence, the Wilson coefficients are the same as in the vacuum case. In the following, we show that the gluon condensates $\phi_{b,c}$ are written in terms of thermodynamic quantities that can be extracted from lattice QCD data.

If we define these condensate terms as

$$G_0(T) = \left\langle \frac{\alpha_s}{\pi} G^a_{\mu\nu} G^{a\mu\nu} \right\rangle_T, \tag{11}$$

$$\left(u^\mu u^\nu - \frac{1}{4} g^{\mu\nu}\right) G_2(T) = \left\langle \frac{\alpha_s}{\pi} G^{a\mu}_{\rho} G^{a\nu\rho} \right\rangle_T, \tag{12}$$

where u^μ is the four-velocity of the medium and taken to be $u^\mu = (1, 0, 0, 0)$, explicit forms of $\phi_{b,c}$ are given as

$$\phi_b = \frac{4\pi^2}{9\big(4m_c^2\big)^2} G_0(T), \tag{13}$$

$$\phi_c = \frac{4\pi^2}{3\big(4m_c^2\big)^2} G_2(T). \tag{14}$$

Actually, it is possible to calculate the condensates [Eqs. (11) and (12)] directly by using lattice QCD, but we do not adopt such an approach here. The gluon condensates generally consist of a perturbative piece and a nonperturbative piece. At zero temperature, the condensate term appearing in QCD sum rules is the nonperturbative piece only and it is shown that the nonperturbative part extracted from lattice QCD by subtracting the perturbative part is indeed consistent with the value of the condensate determined from QCD sum rules for charmonium [30–32]. Similar consideration holds also for the finite temperature case [33], in which we would have to subtract the perturbative part at $T \neq 0$ if we directly calculated the nonperturbative condensates from lattice QCD. In this paper, since we are putting all the temperature dependencies in the condensates, including the perturbative and nonperturbative contributions, we can just extract total temperature dependencies of the operators from the lattice. This is possible by noting that the scalar gluon condensate and twist-2 gluon condensates are, respectively, just the trace part and symmetric traceless part of the energy-momentum tensor. This energy-momentum tensor is well calculated on the lattice from the pressure and energy density of the plasma through the following equation:

$$T^{\alpha\beta} = (\varepsilon + p)\left(u^\alpha u^\beta - \frac{1}{4} g^{\alpha\beta}\right) + \frac{1}{4}(\varepsilon - 3p) g^{\alpha\beta}. \tag{15}$$

The scalar condensate can be related to the trace part through the trace anomaly as

$$T^\mu_\mu = \left\langle \frac{\beta(g)}{2g} G^a_{\mu\nu} G^{a\mu\nu} \right\rangle, \tag{16}$$

with $\beta(g)$ being the beta function, $\beta(g) = -\frac{g^3}{48\pi^2}(33 - 2N_f)$ for one-loop N_f flavors, and N_c colors. Using this expression with $N_f = 0$ and $N_c = 3$ for the beta function and recalling that $T^\mu_\mu = \varepsilon - 3p$, we obtain

$$G_0(T) = G_0^{\rm vac} - \tfrac{8}{11}(\varepsilon - 3p), \tag{17}$$

where $G_0^{\rm vac}$ is the value of the scalar gluon condensate in vacuum [34]. For the twist-2 part, the symmetric traceless part of the energy-momentum tensor is the gluon operator

$$T^{\alpha\beta} = -G^{a\alpha\lambda} G^{a\beta}_{\lambda}. \tag{18}$$

Hence we can identify the traceless part of the energy-momentum tensor to $(\varepsilon + p)$ as given in Eq. (15). From Eq. (12), the twist-2 part becomes

$$G_2(T) = -\frac{\alpha_s(T)}{\pi}(\varepsilon + p), \tag{19}$$

so that $G_2(T)$ is proportional to the entropy density of the system, $s = (\varepsilon + p)/T$. We extract the temperature-dependent quantities ε, p [35], and $\alpha_s(T)$ [29] from lattice calculations for the pure SU(3) system. To construct G_2, we need the temperature-dependent effective coupling constant. The coupling constant, however, cannot be uniquely determined by lattice QCD [29]. In Ref. [29] four kinds of coupling constant were extracted from the color singlet heavy quark-antiquark free energy. Two of them are measured in the short-distance regime and the others are done in the long-distance regime. In the former, one is from the free energy and the other is from the spatial derivative of the free energy (force). Both coupling constants are almost independent of temperature at short distance, $r < 0.1$ fm. Whereas the former goes to a negative value at larger distance owing to the remnant of the confinement force, the latter shows a temperature-dependent maximum value, at which the distance is denoted by $r_{\rm screen}$. Here, we adopt the latter one, $\alpha_{\rm qq}(r, T)$ at $r = r_{\rm screen}$, as one of reasonable coupling constants since it characterizes the relevant length scale for the separation of the short-distance regime from long-distance one. In contrast, the long-distance regime is based on a fit of the free energy to the Debye-screened functional form, which has two coupling parameters: the Coulomb force strength $\alpha(T)$ and screening $\tilde{\alpha}(T)$. Although both of the coupling constants show reasonable temperature dependencies and agree with each other at $T > 6T_c$, we adopt $\tilde{\alpha}(T)$ because the Coulomb force strength is not relevant for characterizing the long-distance nonperturbative physics at the temperature considered here. Unlike $\alpha_{\rm qq}$, the uncertainty in the result of $\tilde{\alpha}(T)$ is too large. Therefore, we use the two-loop

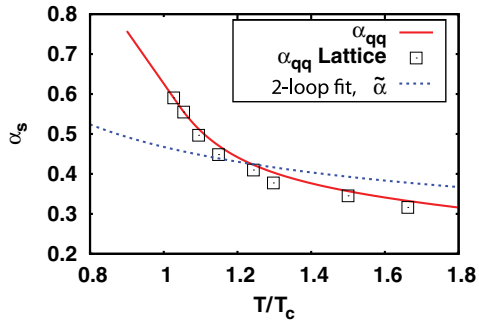

FIG. 1. (Color online) Temperature-dependent coupling constants extracted from lattice QCD. The boxes denote the lattice data points of $\alpha_{qq}(r_{screen}, T)$ taken from Ref. [29]. The solid line is drawn by Bezier interpolation of the lattice data points. The dotted line shows the case of Eq. (20).

perturbative running coupling form

$$g_{\rm pert}^{-2}(T) = \frac{11}{8\pi^2}\ln\left(\frac{2\pi T}{\Lambda_{\overline{\rm MS}}}\right) + \frac{51}{88\pi^2}\ln\left[2\ln\left(\frac{2\pi T}{\Lambda_{\overline{\rm MS}}}\right)\right], \quad (20)$$

with $T_c/\Lambda_{\overline{\rm MS}} \simeq 1.14$, and rescale this as $\tilde{\alpha}(T) = 2.095\alpha_{\rm pert}(T)$ [29]. Here we put $T_c = 264$ MeV [35]. The two coupling constants as a function of temperature are displayed in Fig. 1. As explained later, we will consider only the temperature region near T_c in this paper. Hence, α_{qq} is stronger than $\tilde{\alpha}(T)$ throughout the analyses in this paper.

The resultant gluon condensates G_0 and G_2 for two cases of the coupling constant are shown in Fig. 2.[1] For G_0, we use $G_0^{\rm vac} = (0.35\ {\rm GeV})^4 \simeq 0.015\ {\rm GeV}^4$. We can see that G_0 decreases as temperature increases and reaches less than half of the vacuum value at $T/T_c \simeq 1.04$. It becomes negative at higher temperature but remains positive in the temperature region considered here [33].

C. Moment sum rule for the nuclear medium

In this case, the medium consist of nucleons; thus we do not have to worry about the scattering term. As long as we follow the same method to suppress the contribution from the continuum, we can use the same form of the phenomenological side for the vacuum and finite temperature cases.

Thus, since the medium effect is similarly imposed on the gluon condensates, the difference between the nuclear matter case from that of hot gluonic matter is in the explicit form of $\phi_{b,c}$. To evaluate the expectation value for the ground state of nuclear matter, we employ the linear density approximation [36]

$$\langle O\rangle_{\rm n.m.} = \langle O\rangle_0 + \frac{\rho_N}{2m_N}\langle N|O|N\rangle, \quad (21)$$

where ρ_N and m_N are the normal nuclear matter density and the nucleon mass, respectively. The nucleon state $|N\rangle$ is normalized as $\langle N(p')|N(p)\rangle = 2p_0(2\pi)^3\delta^3(p-p')$. Then, the scalar condensate becomes [21]

$$\left\langle\frac{\alpha_s}{\pi}G^a_{\mu\nu}G^{a\mu\nu}\right\rangle_{\rm n.m.} = \left\langle\frac{\alpha_s}{\pi}G^a_{\mu\nu}G^{a\mu\nu}\right\rangle_0 - \frac{8}{9}m_N^0\rho_N, \quad (22)$$

where $m_N^0 \simeq 750$ MeV is the nucleon mass in the chiral limit [37]. The traceless and symmetric twist-2 operator is given as [21],

$$\left\langle N(p)\left|\frac{\alpha_s}{\pi}G^a_{\alpha\sigma}G^{a\beta\sigma}\right|N(p)\right\rangle = -\left(p_\alpha p^\beta - \frac{1}{4}g_\alpha^\beta p^2\right)\frac{\alpha_s}{\pi}A_G, \quad (23)$$

where A_G is related to the moment of the gluon distribution function,

$$A_G(\mu^2) = 2\int_0^1 dx\, xG(x,\mu^2). \quad (24)$$

Following Ref. [21], we take $A_G(8m_c^2) \simeq 0.9$. Although G_2 at finite temperature is related to the entropy, this correspondence does not hold in the nuclear matter case. Note that Eq. (18) does not contain the quark sector. By using these expressions, the condensate terms that appear in Eq. (5) finally result in [21]

$$\phi_b = \frac{4\pi^2}{9(4m_c^2)^2}\left\langle\frac{\alpha_s}{\pi}G^a_{\mu\nu}G^{a\mu\nu}\right\rangle_{\rm n.m.} \quad (25)$$

$$\phi_c = -\frac{2\pi^2}{3}\frac{\frac{\alpha_s}{\pi}A_G}{(4m_c^2)^2}m_N\rho_N. \quad (26)$$

The form of ϕ_b is the same as for the hot gluonic matter case but now the expectation value is taken through Eq. (22). We depict the density dependence of the gluon condensates based on Eqs. (22) and (26) in Fig. 3. The twist-2 case is renormalized so that it corresponds to the finite temperature case (14). We can see that the change of the scalar condensate reaches as large as that in the $T = T_c$ case at $\rho \sim 5\rho_0$ but is much smaller at normal nuclear density. The twist-2 contribution is much smaller than that of the finite temperature case.

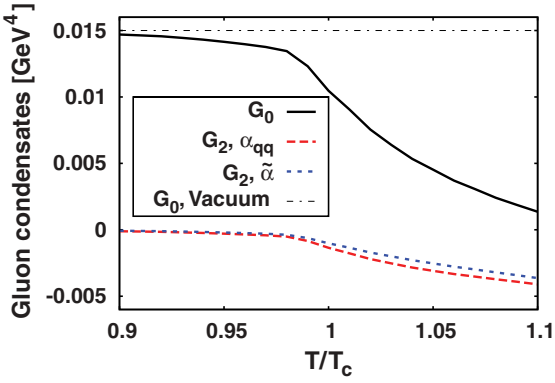

FIG. 2. (Color online) Gluon condensates near T_c.

D. Phenomenological side

On the phenomenological side, we use a simple prescription that describes the lowest lying resonance in each channel. For

[1] We have renewed the extraction from lattice data by improving the resolution, so that the present values are slightly different from those of Ref. [23].

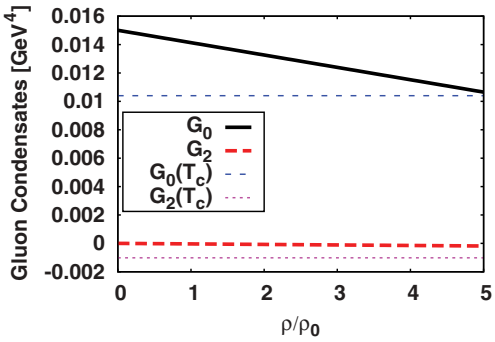

FIG. 3. (Color online) Gluon condensates in nuclear matter. Thick solid and dashed lines show the scalar and twist-2 condensates, respectively, as a function of density normalized by the normal nuclear density. Thin lines are the finite temperature case at $T = T_c$ for a comparison.

charmonium, previous studies [16,19–22] focused on the mass and ignored the small but finite width of J/ψ and η_c. In this case, the imaginary part of the polarization function in Eq. (6) is simply parametrized by

$$\mathrm{Im}\tilde{\Pi}(s) = f_0\delta(s - m^2) + \text{corrections}, \tag{27}$$

where we ignore the channel subscript J. This spectral function immediately leads to the moment

$$M_n(\xi) = \frac{f_0}{\pi(m^2 + Q^2)^{n+1}}[1 + \delta_n(\xi)]. \tag{28}$$

The correction term in Eq. (27) is absorbed in $\delta_n(\xi)$. By taking the ratio as in Eq. (7), we can remove the constant f_0 from the equation. To obtain the mass of the lowest lying resonance, we need to choose sufficiently large n such that $[1 + \delta_{n-1}(\xi)]/[1 + \delta_n(\xi)]$ is close to unity. Then the ratio does not depend on the details of the correction term, which contains higher resonances and continuum, and the mass is simply given by

$$m^2 \simeq \frac{M_{n-1}(\xi)}{M_n(\xi)} - 4m_c^2\xi. \tag{29}$$

Previous analyses rely on this formula.

In this work, we extend this formulation to include finite width. Here, we employ the simple relativistic Breit-Wigner form

$$\mathrm{Im}\tilde{\Pi}(s) = \frac{f_0\sqrt{s}\Gamma}{(s - m^2)^2 + s\Gamma^2} + \text{corrections}. \tag{30}$$

As in the $\Gamma = 0$ case, we can eliminate the unnecessary constant and the effects of the correction term by taking the ratio of the moment and choosing appropriately large n. In the practical analyses of the sum rule, our task is to find values of (m, Γ) that satisfy the sum rule [Eq. (7)]. Generally, there are infinite numbers of the pairs of (m, Γ) because the sum rule provides one equation with respect to the two quantities we want to know. Hence, without additional constraints, the sum rule can provide only a relation between m and Γ as in the case of light vector mesons [38]. Here, before the practical calculation, we discuss the relation between the mass and the width that comes from the phenomenological side, Eq. (30).

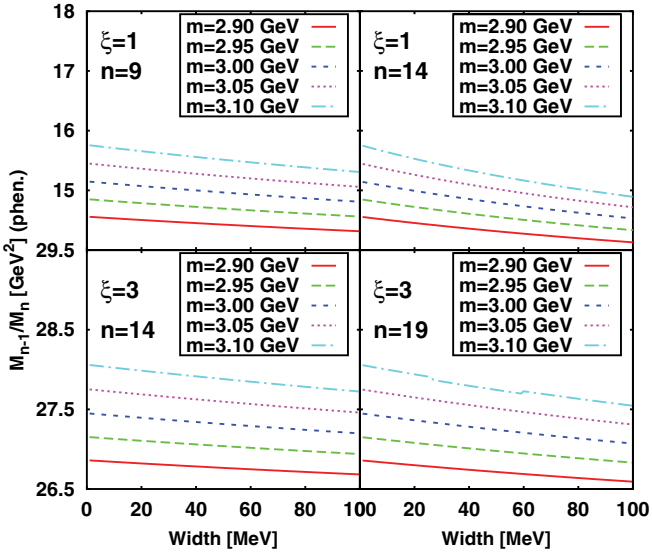

FIG. 4. (Color online) Moment ratio of the phenomenological side as a function of Γ. Upper panels are for $\xi = 1$. Left and right panels denote the cases of $n = 9$ and $n = 14$, respectively. Lower ones are for $\xi = 3$ with $n = 14$ (left) and $n = 19$ (right).

In calculation of the moment ratio of the phenomenological side, we need to compute the dispersion integral in Eq. (6) with the spectral function in Eq. (30). Since the width of ground-state charmonium is much smaller than its mass, we need a careful treatment of the numerical integration. To achieve good accuracy, we performed Monte Carlo integration based on the VEGAS algorithm [39]. In our calculation, the typical relative numerical uncertainty evaluated from the standard manner in the Monte Carlo integration is the order of 10^{-6} for 10^6 events with $m = 3$ GeV and $\Gamma = 1$ MeV. As expected, this accuracy improves as Γ increases.

We plot the Γ dependence of the moment ratio for various mass values from 2.9 to 3.1 GeV in Fig. 4. Here we show the result for two values of ξ, $\xi = 1$ and 3. For each ξ value, we choose two values of n, which are typical values for the analyses in the following, to see the n dependence of the moment ratio. First, comparing the left (smaller n) side to the right (large n) side, we can see that the Γ dependence of the moment ratio becomes stronger as n increases. As we will see later, larger n is suitable for evaluating mass at higher temperature. Hence, this fact means that, as the temperature increases, the system becomes more sensitive to the width. Second, the moment ratio decreases monotonically as the width increases if the mass is unchanged. It also decreases as the mass decreases but the width dependence is much weaker. For instance, let us suppose that we obtain a 1 GeV^2 decrease of the moment ratio from the OPE side for $\xi = 1$. If the mass stays constant, the width must broaden to larger than 100 MeV, whereas it corresponds to about a 100 MeV mass reduction for the case where the width remains at its vacuum value. Finally, as is shown by comparing the upper right with the lower left plots in Fig. 4, the width dependence becomes weaker if we choose larger ξ. Its consequence will be discussed in the next section.

III. CHARMONIUM IN HOT GLUONIC MATTER

In this section, we present the result of the analysis for hot gluonic matter. The parameters of the theory are α_s and m_c. Hereafter, they are set to 0.21 and 1.24 GeV at $\xi = 1$, respectively, which are taken from Ref. [21].

We begin with fixing n such that the moment ratio of the OPE side takes its minimum value for each temperature. As briefly mentioned before, we need to choose moderately large n so that the contributions from excited states and the continuum can be sufficiently suppressed. Therefore, this ratio should approach a constant value at adequately large n. However, on the OPE side contribution from higher dimensional operators will be important at large n. At the n value for which the moment ratio takes its minimum value, pole dominance and truncation of the OPE are valid and the ratio is close to the real asymptotic value, as has been extensively studied in the vacuum case [19].

We display the moment ratio for the OPE side [Eq. (10)] in Figs. 5 and 6 with the gluon condensates shown in Fig. 2.

Figure 5 shows the moment ratio for the vector channel. The left and right columns show the cases in which we use α_{qq} and $\tilde{\alpha}$, respectively. Comparing different ξ cases, we can see that the stability of the moment becomes better as ξ increases. But the values of n that give the stability to the moment ratio also become larger. As previously reported in Ref. [23], the stability is only achieved near T_c and the stronger coupling, which is α_{qq} in this temperature region, gives worse stability. By increasing ξ, we can improve the stability a little. Although stability can be achieved only up to $1.04T_c$ for $\xi = 0$, the moment ratio remains stable up to $1.06T_c$ for $\xi = 3$.

We can see a similar situation in the pseudoscalar channel depicted in Fig. 6. However, the moment ratio is less stable than the vector case. In the pseudoscalar case, even the best case (using $\tilde{\alpha}$ and $\xi = 3$) can stabilize the moment ratio only up to $1.04T_c$.

Note that the lack of stability does not necessarily mean dissociation of the charmonia. The reason for such instability can be clearly seen in the terms of the OPE [Eq. (10)], each of which must be much less than unity for convergence. These terms are displayed in Figs. 7–9. We can see that all the coefficients grow with n. An important feature in all the coefficients is that increasing ξ clearly keeps their value smaller. Among these three, only $c_n(\xi)\phi_c$ always has positive sign and its magnitude increases with temperature. These two features are opposite to $b_n(\xi)\phi_b$, in which the sign is always negative and the value seems to approach zero as temperature increases. In comparing the two channels, one finds that there are no significant differences. Hence, the stability will be determined by a delicate balance among coefficients, and its breakdown will be caused by a rapid increase of $c_n(\xi)\phi_c$.

Now we proceed to the determination of mass and width. The values of n are listed in Table I. Note that the stability achieved at the highest temperature is ambiguous in some cases; for example, J/ψ of $\xi = 2$ with the α_{qq} case is stable at $T/T_c = 1.05$ with $n = 22$. However, as seen in Fig. 5, the moment ratio is almost constant in such a large n region and never rises as lower temperature cases do. Such a vague stability is also seen in other cases. Hence, we note that mass

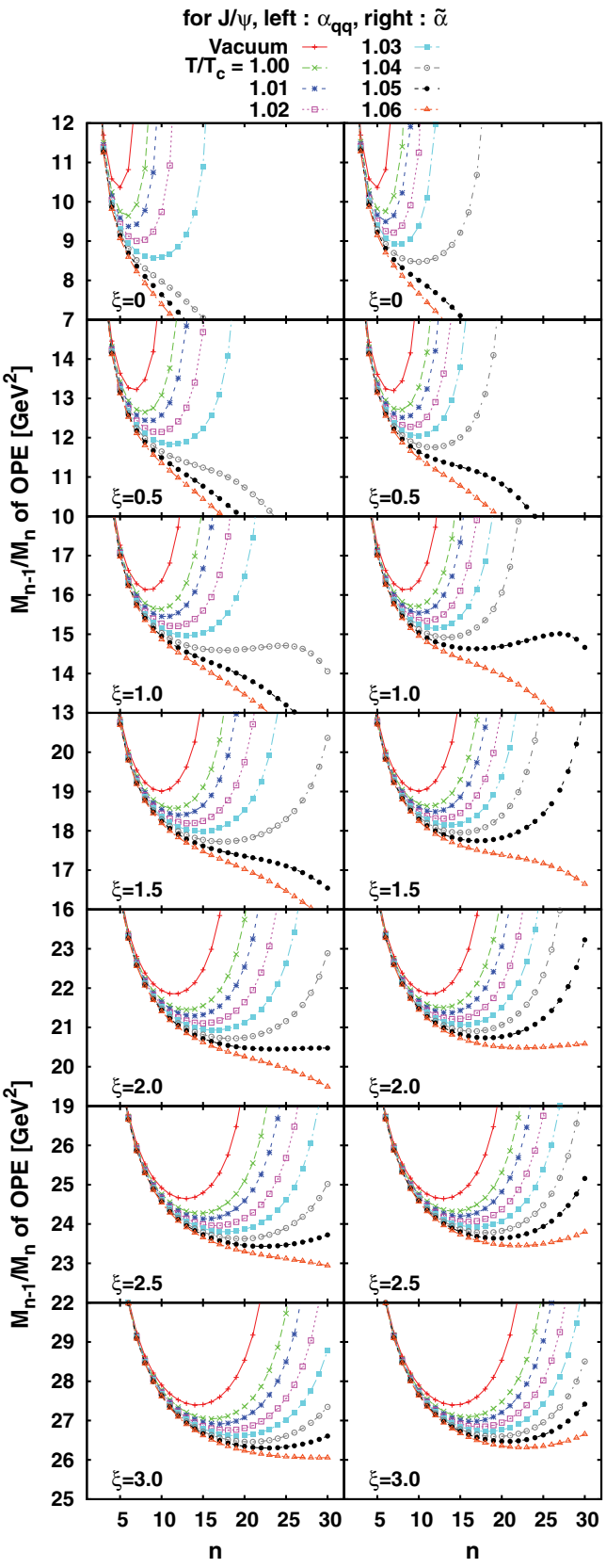

FIG. 5. (Color online) Moment ratio for the OPE side for the vector channel (J/ψ). Each panel shows a different ξ and coupling constant case. The symbols stand for different temperatures.

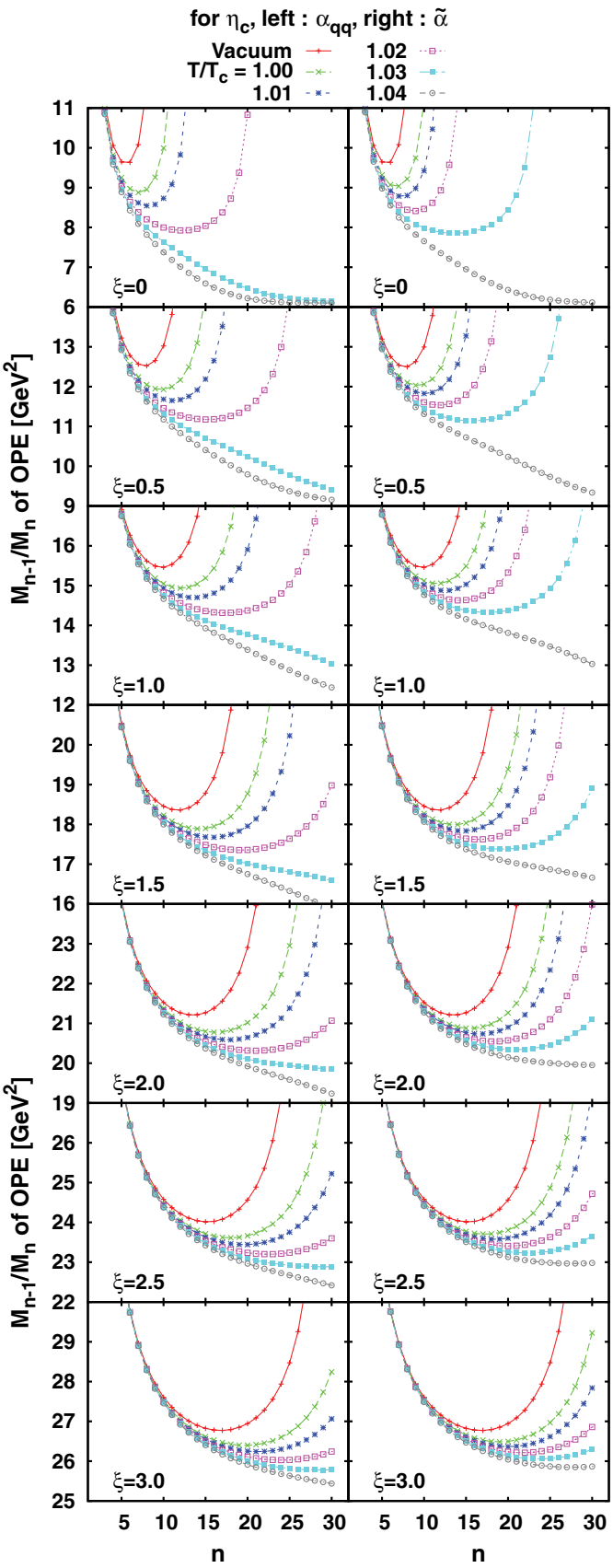

FIG. 6. (Color online) Same as Fig. 5, but for the pseudoscalar channel (η_c).

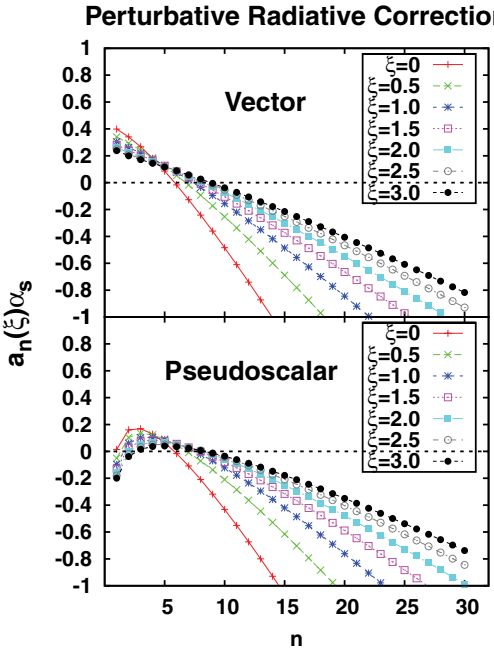

FIG. 7. (Color online) Radiative correction term $a_n(\xi)\alpha_s$ in the OPE. The upper panel shows the vector case and the lower one shows the pseudoscalar case.

and width values evaluated on the basis of such a stability are less reliable in the analyses that follows.

Once n and ξ are fixed, we can compute the mass and the width by making use of Eq. (7). For a fixed moment ratio of the OPE side, we first compute the mass in the limit of $\Gamma \to 0$ using Eq. (29). By virtue of the monotonic behavior of the moment ratio of the phenomenological side shown in Fig. 4, we can safely calculate the mass in the case of finite width by numerically solving Eq. (7) with Eq. (30).

We plot the relation between the mass shift and the width at various temperatures in Figs. 10 and 11. We can see the almost linear behavior of the width as a function of the mass shift. Note that the vacuum mass differs for different ξ. We do not perform fine tuning of the parameters so that the real vacuum mass is reproduced. Although there are some exceptions for the linear relation, especially in small-ξ and high-temperature cases, these come from the vague stability we mentioned before. Hence, we can conclude that the mass shift and the width have the linear relationship provided QCD sum rules work properly. The other important aspect is the temperature dependence of the mass shift and the width. We cannot know how the mass and the width behave in the real situation, since we cannot simultaneously determine both the mass and the width within the current framework. Here, we investigate two extreme cases: the $\Gamma \to 0$ limit and the $\delta m \to 0$ limit.

The results are shown in Figs. 12 and 13. In these figures, we plot the results of $T > 0.9T_c$. Figure 12 shows the remarkable behavior of the mass shift: The mass does not change up to $T \sim T_c$ but it suddenly begins to decrease across T_c. This fact clearly reflects the temperature dependence of the gluon condensates, which represent the phase transition. Above T_c, the mass decreases with temperature almost linearly. This

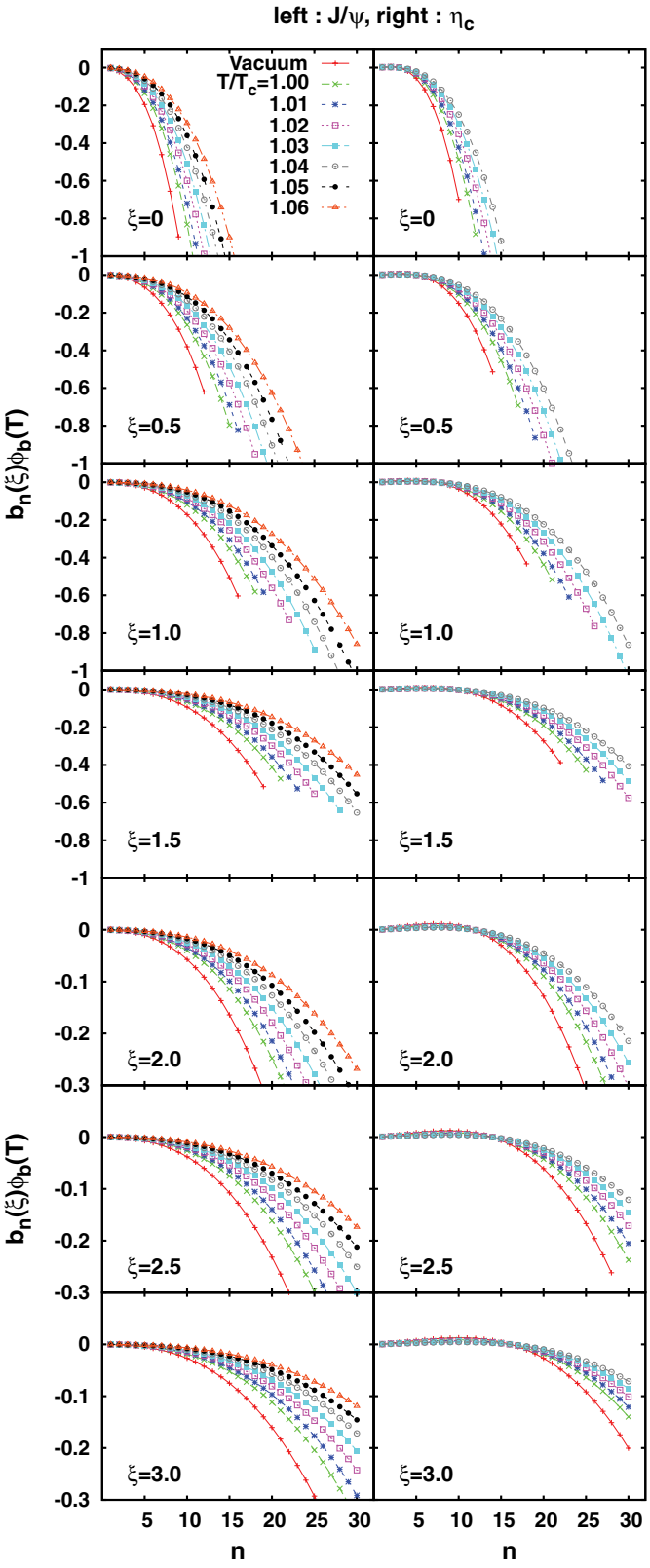

FIG. 8. (Color online) Scalar condensate term $b_n(\xi)\phi_b$. The left and right columns stand for the vector and the pseudoscalar cases, respectively. The symbols denote different temperature cases.

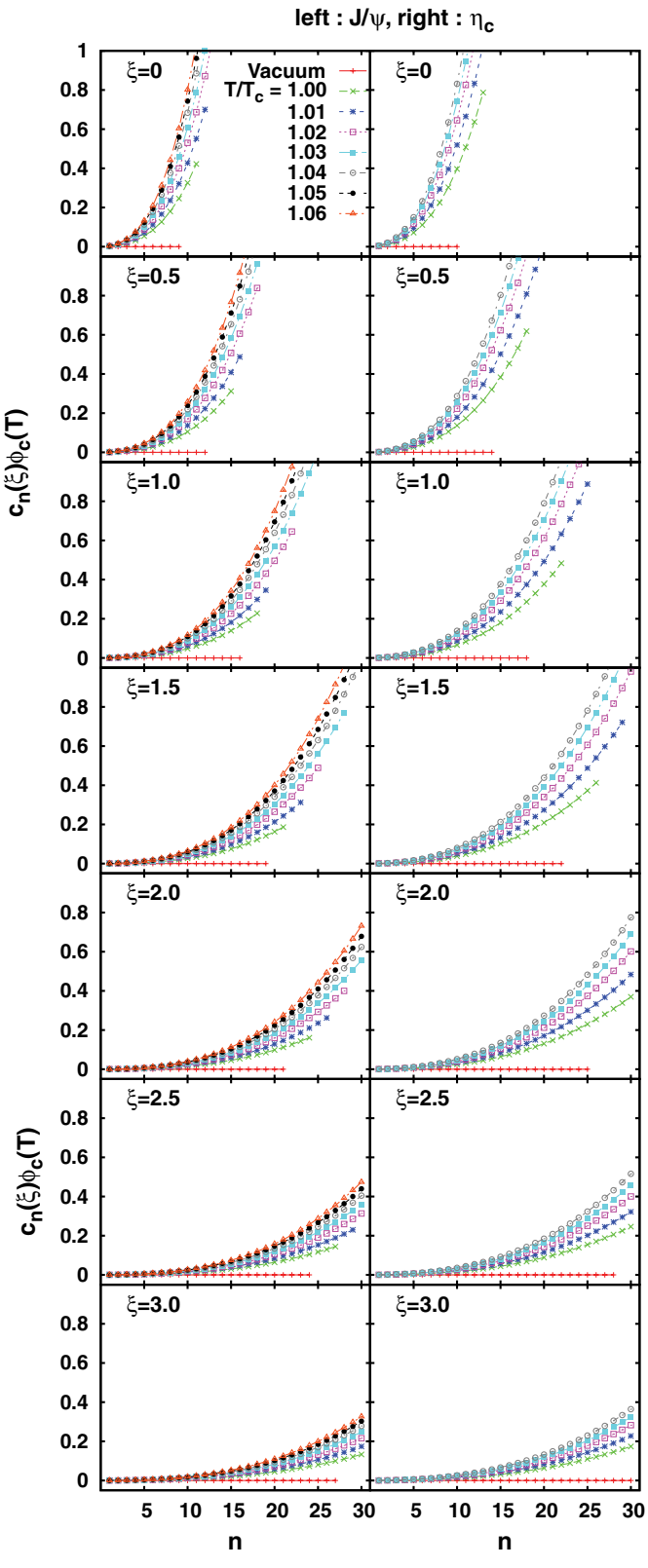

FIG. 9. (Color online) Twist-2 condensate term $c_n(\xi)\phi_c$ with α_{qq}.

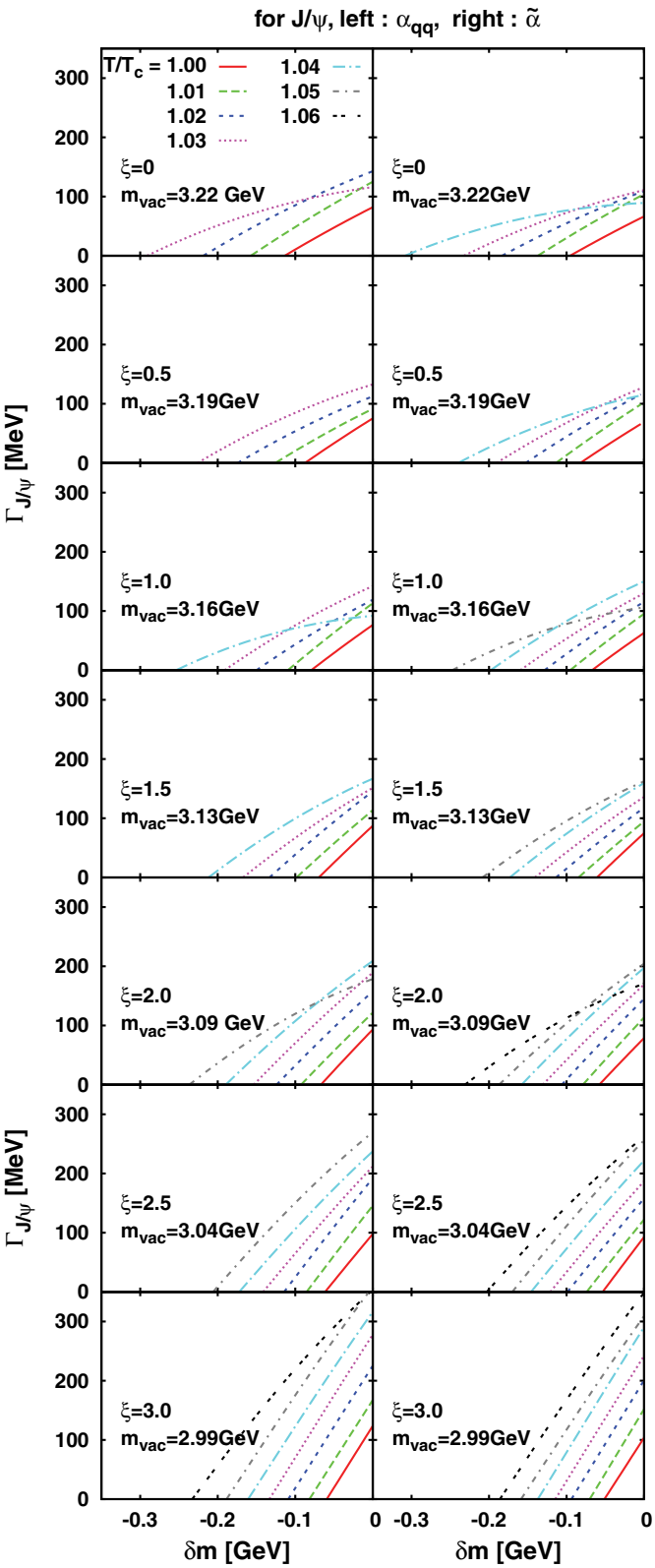

FIG. 10. (Color online) Relation between mass shift $\delta m = m_{\text{vacuum}} - m$ and width Γ for J/ψ. As in Figs. 5 and 6, each figure shows a different ξ case for two cases of the coupling constant, α_{qq} and $\tilde{\alpha}$.

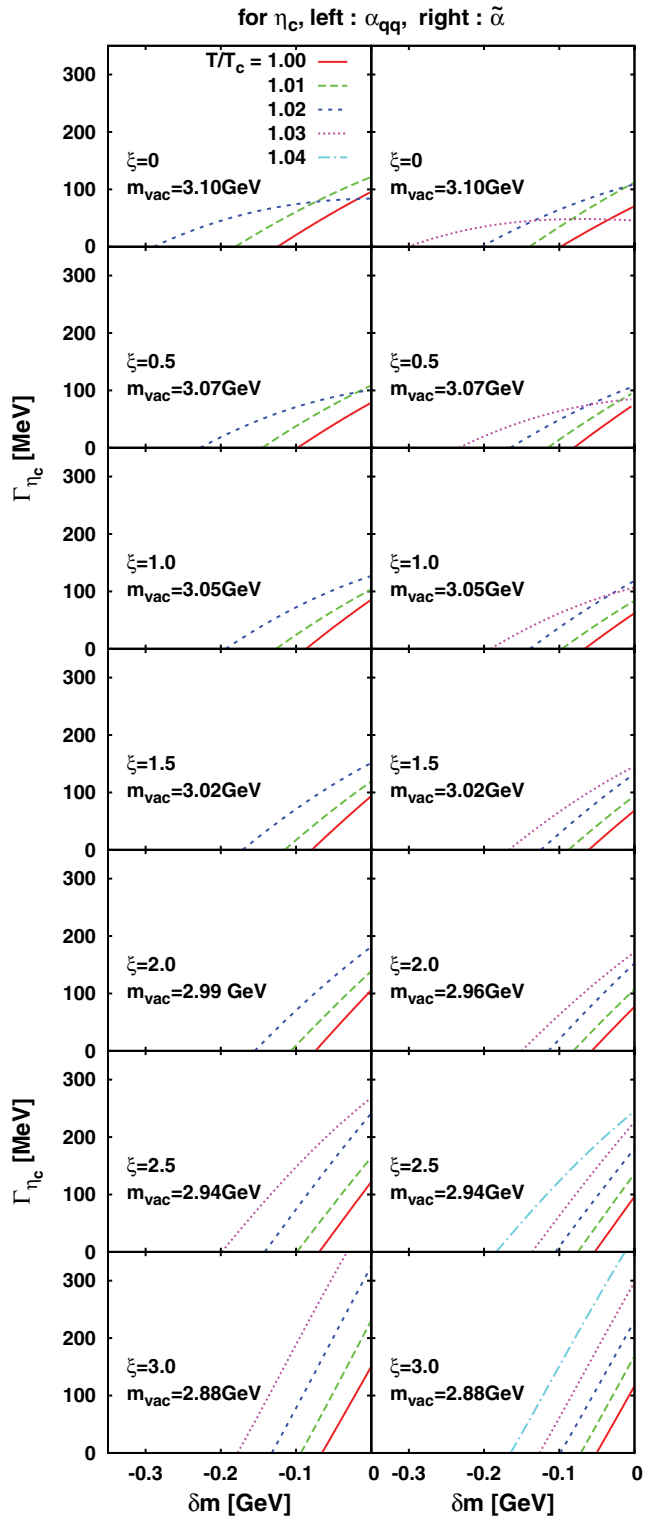

FIG. 11. (Color online) Same as Fig. 10, but for η_c.

feature is common for both J/ψ and η_c. Though small-ξ results, especially those at $\xi = 0$, show a more rapid decrease, the curves become almost parallel among large-ξ results, as a consequence of the better stability. From the nature

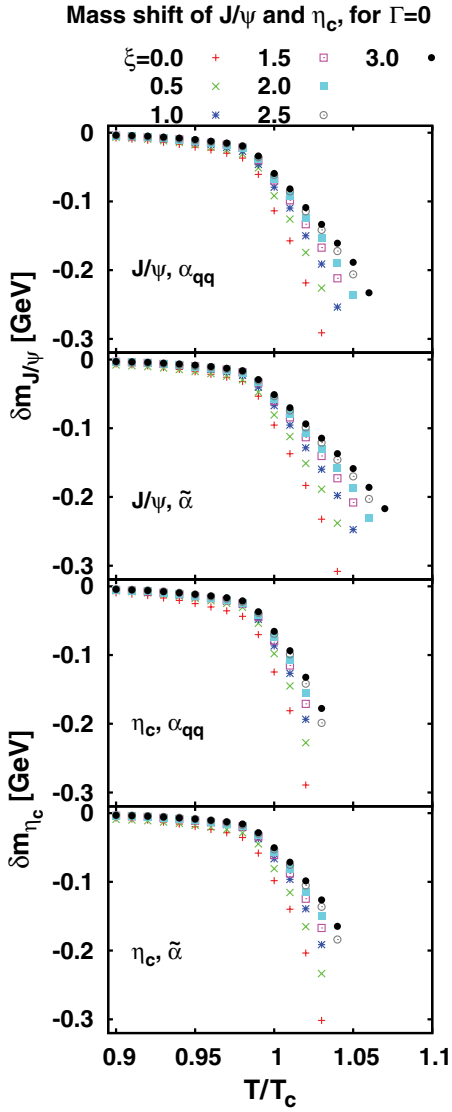

FIG. 12. (Color online) Temperature dependence of the masses in the $\Gamma \to 0$ limit. The symbols stand for different ξ values.

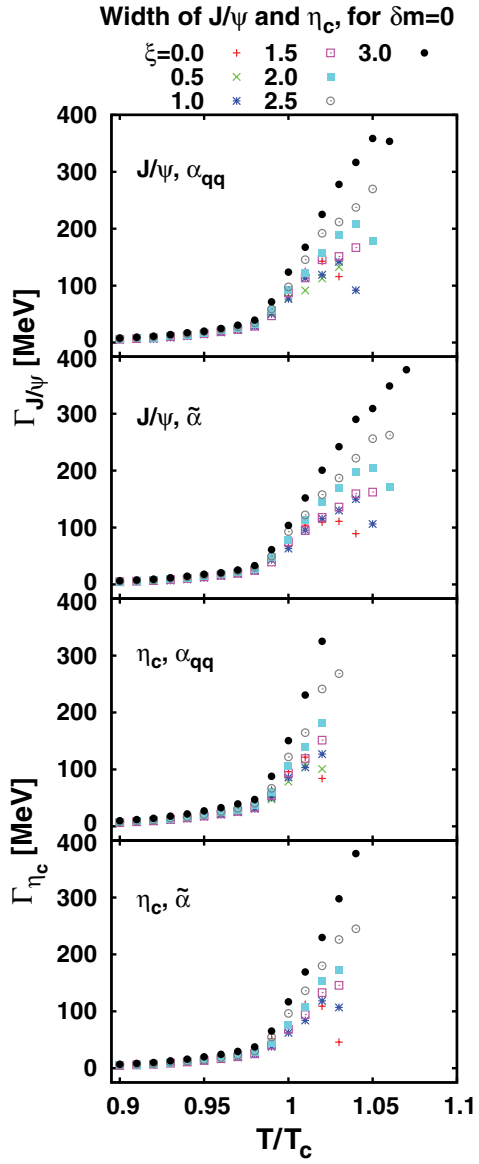

FIG. 13. (Color online) Temperature dependence of the widths in the $m \to 0$ limit. The symbols are the same as in Fig. 12.

of the phenomenological side shown in Fig. 4, this case corresponds to the maximum mass shift. The mass shift shows a reduction of ∼50 MeV from vacuum to T_c, and it increases additionally by ∼20–50 MeV as the temperature rises by $0.01T_c$. Consequently, it becomes 100–300 MeV at $T = 1.04T_c$.

Similarly, Fig. 13 shows that the width begins to increase with temperature across T_c if no mass shift takes place. This also shows an almost linear dependence on temperature above T_c. Though some exceptions can be seen in the small-ξ results, which are also indicated in Figs. 10 and 11, these behaviors come from the vague stability appearing at the too large n values in Table I. Hence, we can conclude that the width increases linearly with temperature above T_c if the mass remains unchanged. Since we did not fine tune the parameters for each ξ, the values of mass shift and width differ for different ξ. However, the qualitative features do not depend on ξ where the stability is reliable. This shows the robustness of our analysis. A realistic change at each temperature should be a combined decrease in mass and an increase in width, whose values are smaller than their maximal changes obtained here. However, to determine a realistic combination, we need to have an additional constraint between the changes in the width and the mass or input the thermal width from another calculation.[2] From Fig. 2, one may think that the dominant contribution to the change of mass and/or width is the scalar gluon condensate, which exhibits a sudden decrease around T_c. However, G_2 also exhibits similar behavior since it is related to the entropy density. Though the value of G_2 around T_c is smaller than G_0 because of the prefactor α_s/π, the relative contribution to the moment becomes larger as T increases. To see the contribution clearly, we show the mass shift of J/ψ

[2]See Ref. [40] for a recent investigation.

TABLE I. List of n values at which the moment ratio takes minimum values.

J	$\alpha_s(T)$	ξ	Vacuum	$\frac{T}{T_c}=1$	1.01	1.02	1.03	1.04	1.05	1.06
J/ψ	α_{qq}	0	5	6	6	7	9	N/A[a]	N/A	N/A
		0.5	7	8	9	10	11	N/A	N/A	N/A
		1	8	10	10	12	13	N/A	N/A	N/A
		1.5	10	11	12	13	15	17	N/A	N/A
		2	11	13	14	15	16	18	23	N/A
		2.5	13	15	15	16	18	20	22	N/A
		3	14	16	17	18	19	21	23	29
	$\tilde{\alpha}$	0	5	6	6	7	8	10	N/A	N/A
		0.5	7	8	8	9	10	12	N/A	N/A
		1	8	10	10	11	12	13	17	N/A
		1.5	10	11	12	13	14	15	17	N/A
		2	11	13	13	14	15	16	18	23
		2.5	13	14	15	16	17	18	19	22
		3	14	16	16	17	18	19	21	23
η_c	α_{qq}	0	6	7	8	12	N/A	N/A	N/A	N/A
		0.5	8	10	11	15	N/A	N/A	N/A	N/A
		1	10	12	14	17	N/A	N/A	N/A	N/A
		1.5	12	14	16	19	N/A	N/A	N/A	N/A
		2	14	16	18	21	N/A	N/A	N/A	N/A
		2.5	15	18	20	22	29	N/A	N/A	N/A
		3	17	20	21	24	29	N/A	N/A	N/A
	$\tilde{\alpha}$	0	6	7	7	9	14	N/A	N/A	N/A
		0.5	8	9	10	12	16	N/A	N/A	N/A
		1	10	12	13	14	18	N/A	N/A	N/A
		1.5	12	14	15	16	19	N/A	N/A	N/A
		2	14	16	17	18	21	N/A	N/A	N/A
		2.5	15	17	18	20	22	28	N/A	N/A
		3	17	19	20	22	24	28	N/A	N/A

[a]N/A means the stability is not available.

without the G_2 term for $\xi = 1$ together with the two different coupling cases in Fig. 14. We can see that almost half of the mass shift is caused by the decrease of G_2. Clearly, a larger G_2 value in which α_{qq} is adopted as the coupling constant leads to a larger mass shift. At $T = 1.04T_c$, α_{qq} is about 25% larger than $\tilde{\alpha}$. This difference makes the mass shift 30 MeV larger in the $\xi = 1$ case. Unfortunately, the present analysis is limited to the temperature region around T_c; the role of the twist-2 term will become more important at higher temperature.

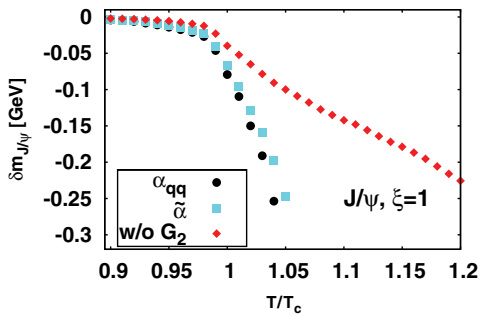

FIG. 14. (Color online) δm of J/ψ without the twist-2 term G_2. See text for details.

IV. NUCLEAR MATTER

In this section, we analyze change of mass and width of the charmonium induced by the nuclear medium within the same framework that was implemented in the previous section. Here, we use Eqs. (25) and (26) instead of Eqs. (13) and (14), respectively. With the common parameter set, the condensates are $\phi_b = 1.74 \times 10^{-3}$ for vacuum, 1.64×10^{-3} for nuclear matter, and $\phi_c = -1.28 \times 10^{-5}$.

As previously shown in Ref. [21], the change of mass, which is identical to the change of the moment ratio of the OPE side [Eq. (29)], is not as large as in the hot gluonic matter case. Thus we do not have to worry about the stability of the OPE. Nevertheless, increasing ξ improves the validity of the OPE. We will show the results for $0 \leqslant \xi \leqslant 3$ as well as in the hot gluonic matter case to show the robustness and the consistency of the calculation.

We list in Table II values of n in which the moment ratio of the OPE side for the nuclear medium becomes minimum. The vacuum case has been already shown in Table I. Comparing these two cases, we can see that the values of n are the same except for a few J/ψ cases, by virtue of the small shift of the gluon condensates in the nuclear matter. In such exceptional cases, the difference of the values of the moment ratio from

TABLE II. List of n values that stabilize the moment ratio for nuclear matter.

Channel	$\xi = 0$	$\xi = 0.5$	$\xi = 1$	$\xi = 1.5$	$\xi = 2$	$\xi = 2.5$	$\xi = 3$
J/ψ	5	7	9	10	12	13	14
η_c	6	8	10	12	14	15	17

the same vacuum case n value is almost negligible (i.e., the moment ratio is almost constant around these n).

We plot the width Γ as a function of the mass shift δm in Fig. 15 as well as in the GP case. In both J/ψ and η_c cases, values of ξ smaller than 1.5 show a larger mass shift and width broadening but larger ξ results agree each other. From the stability argument, larger ξ results will be more reliable. Then, possible mass shifts are maximally -7 MeV for J/ψ and -4 MeV η_c whereas maximum widths are 10 MeV for J/ψ and 6 MeV for η_c.

V. DISCUSSION AND SUMMARY

In Sec. III, we have shown that mass decreases suddenly across T_c and the shift reaches maximally a few hundred MeV above T_c in hot gluonic matter. Alternatively, width can also maximally broaden to $\sim$200 MeV. Although our analysis cannot determine both of mass and width simultaneously, this is a notable result that should be examined in future experiments. In fact, a next-to-leading-order QCD calculation shows that the thermal width of J/ψ slightly above T_c is smaller than a few 10 MeV [41,42]. Hence a large mass shift will take place. Note that such a large mass shift has been expected from different points view; an AdS/QCD analysis shows a sudden drop of mass at the phase transition [43]. In Ref. [43], although the mass begins to slowly increase at higher temperature, the temperature region investigated in the present paper corresponds to the critical region. A sudden reduction of the asymptotic value of the potential seen in lattice QCD [44] leads to a lowering of the bound-state energy [45]. Recent

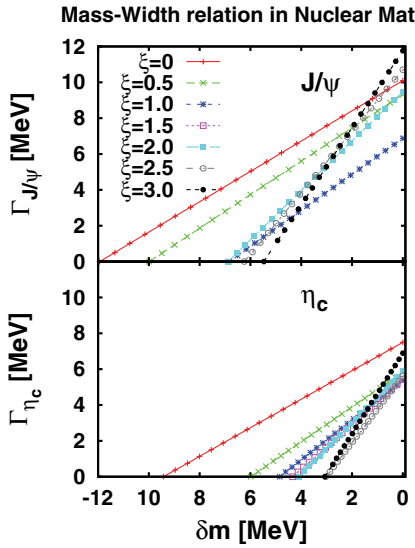

FIG. 15. (Color online) Relation between mass shift and width in nuclear matter.

lattice QCD calculations based on the maximum entropy method also show survival of the peak in the spectral function above T_c [46] but the resolution is still insufficient to allow discussion of the shift and broadening of the peak. Since our results access only the region near T_c, we are still far from a complete understanding of the behavior of the charmonium in the deconfined medium. In the most plausible picture from our current understanding, charmonia are melting at the very high temperature expected in the early stage of the heavy-ion collisions at RHIC and LHC. Then the pairs of heavy quark and antiquark form the bound states at a certain temperature, which depends on quantum number. The temperature is expected as $\sim 2T_c$ for J/ψ at RHIC [47]. After charmonia are produced, they will dissociate by collisions with partons. If this phase lasts long enough compared to the inverse of the width, the charmonia can decay in the medium. In fact, the lifetime of the partonic medium is about 4–5 fm/c in a hydrodynamic calculation for the central Au+Au collisions at the maximum RHIC energy [48]. This will be much longer at LHC. From Fig. 10, we expect an $\sim$200 MeV J/ψ mass reduction in the case of the small decay width. This shift is larger than the experimental mass resolutions ($\sim$35 MeV for the dielectron channel of PHENIX at RHIC [8] and 33 MeV for the dielectron channel and 75 MeV for the dimuon channel of ALICE at LHC [49]).

Alternatively, statistical hadronization near the phase boundary has also been examined [50]. In this case, the number of produced charmonia will be enhanced if a notable mass shift occurs. For example, there may be a factor of 2 enhancement for $T = 170$ MeV and $\delta m = -100$ MeV since the enhancement factor is given by $e^{-\delta m/T}$. This enhancement might be observed by comparing particle ratio.

For the nuclear medium result, we have extended the analysis carried out in Ref. [21] by taking account of finite width. We have also shown the results for different ξ values. Since we have given the relation between the mass shift and width, we can estimate the mass shift in the presence of a finite width effect by considering the dissociation cross section of the charmonium by a nucleon. Provided the Fermi momentum is $p_F \simeq 250$ MeV and the cross section is $\sigma_{J/\psi-N} \simeq 2$ mb, the decay width $\Gamma = \langle \sigma_{J/\psi-N} v_{\rm rel} \rho_N \rangle$ becomes $\sim$1.3 MeV for charmonium at rest. The cross section may be smaller, because the incident momentum is considered to be small and the process will be near threshold. From this estimate, if we take into account the broadening of the width, the mass shift becomes slightly smaller, by about 0.5 MeV, according to the results shown in Fig. 15. Therefore, this justifies the argument in Ref. [21] that the influence of the decay widths is expected to be small.

The change of spectral properties in nuclear matter can be experimentally investigated by the Panda experiment

at GSI-FAIR in which incident antiprotons collide with a nuclear target. Here we present some predictions for cross sections of charmonium production through $\bar{p}p$ annihilation and subsequent decay into dileptons or radiative decay in the experiment. We compute the cross sections with the Breit-Wigner formula

$$\sigma_{\rm BW}(s) = \frac{B_{\rm in}B_{\rm out}(2J+1)}{(2s_1+1)(2s_2+1)}\frac{4\pi}{k_{\rm cm}^2}\frac{s\Gamma_{\rm tot}^2}{(s-m^2)^2+s\Gamma_{\rm tot+med}^2} \quad (31)$$

where s, $k_{\rm cm}^2$, and m are the Mandelstam variable, c.m. momentum, and mass of charmonium with spin J, respectively; $\Gamma_{\rm tot}$ is the total decay width of the charmonium and $\Gamma_{\rm tot+med} = \Gamma_{\rm tot} + \Gamma_{\rm medium}$; $B_{\rm in}$ and $B_{\rm out}$ are the branching fraction of the resonance into the entrance and exit channels, respectively; and s_i is the spin of the incident particles, which are antiprotons and protons in the present calculation. Since the target protons are in the nucleus, we have to take the Fermi motion into account for accurate estimation. We average the Breit-Wigner cross section with respect to the target momentum as

$$\overline{\sigma_{\rm BW}} = \frac{4}{\rho_0}\int_0^{k_F} k^2\frac{dkd\Omega}{(2\pi)^3}\sigma_{\rm BW}. \quad (32)$$

In addition to J/ψ and η_c, we also calculate cross sections for χ_c, which are expected to show larger mass shifts, with $\delta m \simeq -40$ to -60 MeV [51]. The parameters in the calculations are summarized in Table III. $\Gamma_{\rm medium}$ is treated as a free parameter varied from 1 to 20 MeV.

Results of the cross sections as a function of incident antiproton energy are shown in Figs. 16–20. We can clearly see that sharp peaks of the resonances disappear. This is because of the Fermi motion of the target protons in the nucleus. For example, an incident energy to create J/ψ (3097) is $E_{\rm lab} = 4.17$ GeV, but the fluctuation of the target momentum makes it possible to create J/ψ with $3.17 \leqslant E_{\rm lab} \leqslant 5.51$ GeV, in which the minimum and the maximum $E_{\rm lab}$ correspond to the target momenta along the collision axis of $p_{2z} = -k_F$ and k_F, respectively. This effect considerably broadens the cross section. Consequently, one needs no fine tuning of incident proton energy to produce charmonium. For J/ψ and η_c, mass shifts are so small that the peak positions of incident energy do not change. However, a mass shift of $\chi_c \sim -60$ MeV is sufficiently large to show a clear shift of the peak in the cross section. In these calculations, we treat $\Gamma_{\rm medium}$ as a free parameter. It is shown that this parameter affects only the magnitude of the cross section, which is larger for smaller change from the vacuum width. Hence, though we cannot predict both the mass shift and the in-medium width, we can obtain information on both quantities from the experimentally measured cross sections. We summarize the cross sections and expected event rate at GSI-FAIR, the luminosity of which is expected to be 2×10^{32} cm^{-2} s^{-1}, in the last two column of Table III. We can see that the expected event rates are large enough for the mass shift of χ_c to be observed.

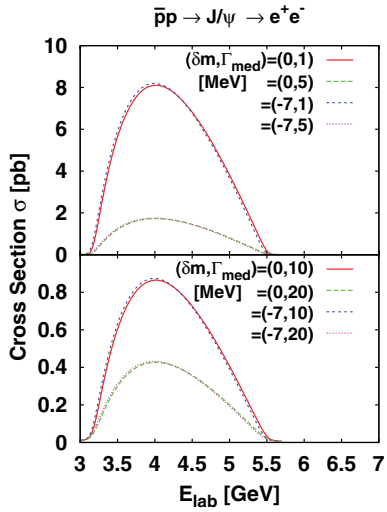

FIG. 16. (Color online) Cross section of J/ψ production in $\bar{p}$-A collisions. The upper panel shows smaller medium width (1- and 5-MeV) cases and the lower one shows larger (10- and 20-MeV) cases with and without mass shift.

Finally, we address possible improvements of this work. Since we restricted ourselves to a hot medium consisting of gluons only in the first part of this paper, we should take the quarks into account for a more realistic estimation.

To consider the quark effects, first we consider the quark operators appearing on the OPE side. We can neglect the light-quark contribution to the OPE, because the light-quark operators appear in the OPE at order $\alpha_s^2(q^2)$: This is why the light-quark condensate can be neglected in the sum rules for a heavy-quark system. However, thermal heavy quarks that directly couple to the heavy-quark current contribute to the OPE at leading order. This is different from the heavy-quark condensates that are perturbatively generated from the gluon condensates and contribute to the OPE through gluon condensates, whose Wilson coefficients are calculated in the momentum representation. The direct thermal quark contributions are called the scattering terms. However, similar terms also appear on the phenomenological side, which also

TABLE III. Parameters and results in charmonium productions at GSI-FAIR. Cross sections and event per day correspond to the case of maximum medium width, $\Gamma_{\rm med} = 20$ MeV.

Resonance	m (MeV)	δm (MeV)	$\Gamma_{\rm tot}$	Final state	$\overline{\sigma_{\rm BW}}$ at peak (pb)	Events per day
J/ψ	3097	−7	93.4 keV	$e^+ + e^-$	0.435	7.5
η_c	2980	−4	25.5 MeV	$e^+ + e^-$	10.7	184
χ_{c0}	3415	−60	10.4 MeV	$J/\psi + \gamma$	18.0	311
χ_{c1}	3511	−60	0.89 MeV	$J/\psi + \gamma$	4.5	78
χ_{c2}	3556	−60	2.05 MeV	$J/\psi + \gamma$	19.8	343

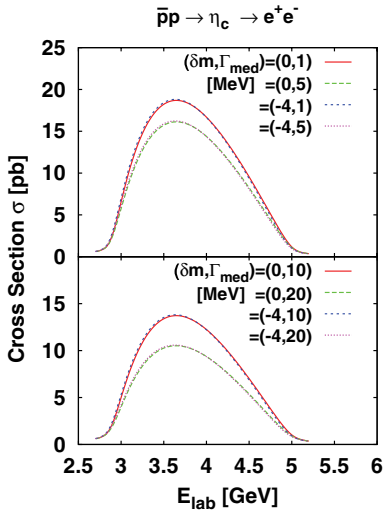

FIG. 17. (Color online) Same as Fig. 16, but for η_c.

has a free charm quark mode that is not coupled with a light quark in the form of a D meson above T_c, as been recently studied in Ref. [52]. Therefore, the scattering term will cancel out between the OPE side and the phenomenological side in the deconfined medium.

Second, the gluon condensates themselves can have a different temperature dependence in the presence of dynamical quarks. As discussed before, the important input for the mass and width change is the temperature dependence of gluon condensates in Fig. 2; in particular the dominant contribution comes from the temperature dependence of G_0. For that purpose, we note that the trace of the energy-momentum tensor to leading order is given as

$$T^{\mu}_{\mu} = -\left(\frac{11-2/3N_f}{8}\right)\left\langle \frac{\alpha_s}{\pi} G^a_{\mu\nu} G^{a\mu\nu}\right\rangle + \sum_q m_q \langle \bar{q} q\rangle. \quad (33)$$

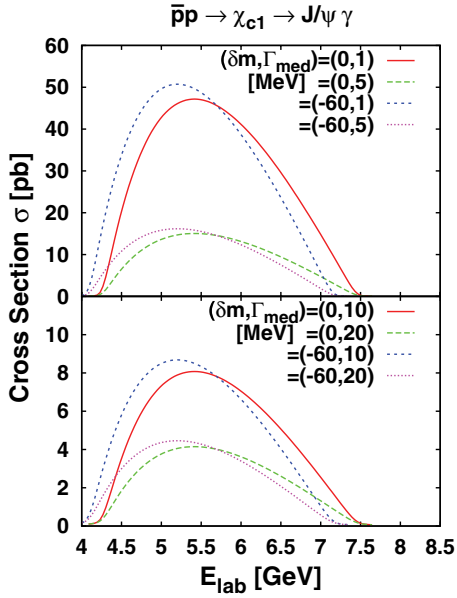

FIG. 19. (Color online) Same as Fig. 16, but for χ_{c1}.

Therefore, we start from the lattice calculation of the trace of the energy-momentum tensor for the full QCD with realistic quark masses given in Ref. [53]. Then, we subtract the fermionic part of the trace anomaly, which was also shown in the literature, from the total. Next, we divide the result for the relevant prefactor with $N_f = 3$, multiplying the gluon condensate as given in Eq. (33). Since the critical temperature T_c differs, we compared it as a function of T/T_c in which $T_c = 196$ MeV for the full QCD case [53]. As can be seen in Fig. 21, the magnitudes of the resulting change near the critical temperature are remarkably similar for the full and pure gluon QCD; although the slope at T_c is milder for full QCD as a consequence of the rapid cross-over transition instead of the

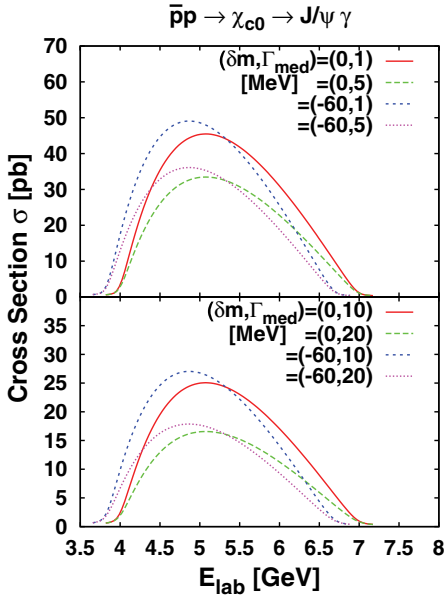

FIG. 18. (Color online) Same as Fig. 16, but for χ_{c0}.

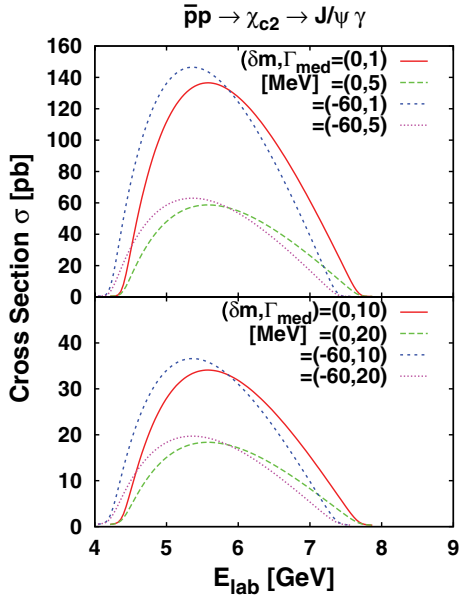

FIG. 20. (Color online) Same as Fig. 16, but for χ_{c2}.

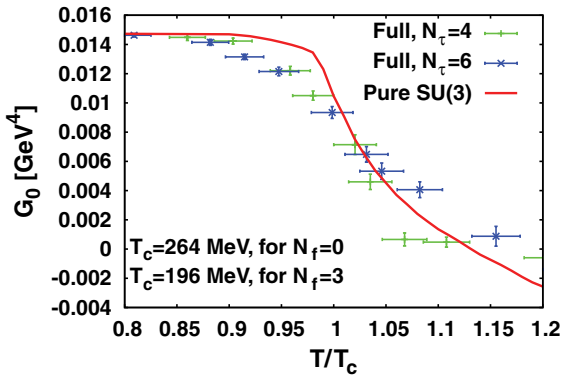

FIG. 21. (Color online) Comparison of the scalar gluon condensate in pure gauge theory with the one of full QCD. Horizontal error bars in the full QCD case are drawn by assuming the 2% uncertainty in the conversion from the lattice units to physical temperature [53].

first-order phase transition. Since the change of the condensate sets in at a lower T/T_c in the full QCD case, the mass and width of charmonia might start varying at a lower temperature in a realistic case than in pure glue theory. For the twist-2 condensates, the results will be less affected by taking into account the fermionic part since the effect will be small in this temperature region. Therefore we believe our main argument and the quantitative result will not be altered even in a realistic situation.

It is also important to study the change of χ_c at finite temperature, which may influence the quantitative feature of the sequential melting [54], since the non-negligible fraction of J/ψ comes from the decay of ψ' and χ_c in relativistic heavy-ion collisions. This can be done by calculating Wilson coefficients for tensor operators for these channels. It should also be noted that the continuum part of the spectral function may play an important role. This will be possible by modeling the medium with a gas of quasiparticles. One more thing to be done is to extend the study to higher temperature. The failure of $T > 1.06T_c$ for J/ψ and $T > 1.04T_c$ for η_c originates from the instability of the moment ratio of the OPE side. The twist-2 gluon condensates becomes larger as temperature increases and then leads to the breakdown of the stability on the OPE side, including up to dimension four (see Fig. 9) and $\mathcal{O}(\alpha_s)$. In Fig. 7, we can also see that the expansion is not good at the large n values that stabilize the moment ratio at higher temperature. These facts suggest the necessity of including higher dimensional operators, which is examined in Ref. [55]. However, we do not know a simple way to extract the temperature dependencies of the higher dimensional operators from the lattice calculation, as was done in the present work for dimension-four operators. The other way to extend this study is to improve the phenomenological side by including a temperature-dependent continuum contribution. The decrease of the scalar gluon condensates above T_c indicates that a perturbative contribution becomes more important at higher temperature. If we can construct a more appropriate phenomenological side reflecting the nature of the strongly interacting matter, this will lead to n-independent results for physical parameters until the charmonia really dissolve.

We also note that there are some opportunities to improve the analyses for nuclear matter. The present analysis shows that the mass shift of χ_c states are likely to be observed in forthcoming experiments. However, the current estimate of the mass shift is not a decisive one; we have to take the twist-2 contribution into account for a more accurate estimation.

In summary, we have given a comprehensive analysis of medium-induced change of the spectral properties of J/ψ and η_c in the hot gluonic medium and the nuclear medium by making use of QCD sum rules. In the case of the gluonic medium, our analysis shows that there must be a notable change of mass or width, or both around T_c, caused by the rapid change of the gluon condensates. Although the present formalism is found to be applicable only up to $T \simeq 1.06T_c$, the change of mass and width can maximally reach a few hundred MeV. We have discussed its implication for the future heavy-ion experiment at CERN-LHC. For the nuclear matter case, we extend the past work to include small but finite width and check the robustness by varying the scale parameter of the theory. We also examined the possibility of detecting such mass shifts in the future experiment at GSI-FAIR. Although J/ψ and η_c do not show prominent signals, χ_c exhibits more promising results. These analyses will provide the basis for future improvements in studying the nature of the strongly interacting matter deeply with charmonia.

ACKNOWLEDGMENTS

K.M. would like to thank the members of the high-energy-physics group of Waseda University for allowing him to use their workstations. We also would like to acknowledge T. Hatsuda for his fruitful comments and discussions. This work was supported by the BK21 Program of the Korean Ministry of Education. S.H.L. was supported by the Korean Research Foundation KRF-2006-C00011 and by the Yonsei University research fund.

APPENDIX: WILSON COEFFICIENTS

Here we list explicit forms of the Wilson coefficients that appear in Eq. (10) and are originally given in Refs. [19] and [21]. In the following, $\rho = \xi/(1+\xi)$ and $F(a,b,c;x)$ is the hypergeometric function ${}_2F_1(a,b,c;x)$.

For the pseudoscalar channel,

$$A_n^P(\xi) = \frac{3}{8\pi^2}\frac{2^n(n-1)!}{(2n+1)!!}(4m^2)^{-n}(1+\xi)^{-n} \times F(n,1/2,n+3/2;\rho), \tag{A1}$$

$$a_n^P(\xi) = \frac{(2n+1)!!}{3\cdot 2^{n-1}n!}\left[\pi - \frac{1}{2(n+1)}\left(\frac{1}{2}\pi - \frac{3}{4\pi}\right) \times F(n,1,n+2;\rho)\right]\frac{1}{F(n,1/2,n+3/2;\rho)} - \left(\frac{1}{2}\pi - \frac{3}{4\pi}\right)$$

$$+\frac{1}{\pi}\left[\frac{8}{3}-\frac{4}{n}\frac{F(n,3/2,n+3/2;\rho)}{F(n,1/2,n+3/2;\rho)}\right.$$
$$\left.-\frac{5}{6}\frac{1}{n+3/2}\frac{F(n,3/2,n+5/2;\rho)}{F(n,1/2,n+3/2;\rho)}\right]$$
$$-2n\frac{\ln(2+\xi)}{\pi}\frac{(2+\xi)}{(1+\xi)^2}\frac{F(n+1,1/2,n+3/2;\rho)}{F(n,1/2,n+3/2;\rho)}, \quad \text{(A2)}$$

$$b_n^P(\xi)=-\frac{n(n+1)(n+2)(n+3)}{2n+3}(1+\xi)^{-1}$$
$$\times\left[\frac{F(n+1,-3/2,n+5/2;\rho)}{F(n,1/2,n+3/2;\rho)}\right.$$
$$\left.-\frac{6}{n+3}\frac{F(n+1,-1/2,n+5/2;\rho)}{F(n,1/2,n+3/2;\rho)}\right], \quad \text{(A3)}$$

$$c_n^P(\xi)=b_n^P(\xi)-\frac{4n(n+1)}{(1+\xi)}\frac{F(n+1,-1/2,n+3/2;\rho)}{F(n,1/2,n+3/2;\rho)}. \quad \text{(A4)}$$

Similarly, for the vector channel,

$$A_n^V(\xi)=\frac{3}{4\pi^2}\frac{2^n(n+1)(n-1)!}{(2n+3)!!}\frac{F(n,1/2,n+5/2;\rho)}{[(4m^2)(1+\xi)]^n}, \quad \text{(A5)}$$

$$a_n^V(\xi)=\frac{(2n+1)!!}{3\cdot 2^{n-1}n!F(n,1/2,n+5/2;\rho)}\left(\frac{2n+3}{2n+2}\right)$$
$$\times\left\{\pi-\left[\frac{\pi}{3}+\frac{1}{2}\left(\frac{\pi}{2}-\frac{3}{4\pi}\right)\right]\frac{F(n,1,n+2;\rho)}{n+1}\right.$$
$$\left.+\frac{F(n,2,n+3;\rho)}{3(n+1)(n+2)}\left(\frac{\pi}{2}-\frac{3}{4\pi}\right)\right\}-\left(\frac{\pi}{2}-\frac{3}{4\pi}\right)$$
$$-2n\frac{\ln(2+\xi)}{\pi}\frac{(2+\xi)}{(1+\xi)^2}\frac{F(n+1,1/2,n+7/2;\rho)}{F(n,1/2,n+5/2;\rho)}, \quad \text{(A6)}$$

$$b_n^V(\xi)=-\frac{n(n+1)(n+2)(n+3)}{(2n+5)(1+\xi)^2}$$
$$\times\frac{F(n+2,-1/2,n+7/2;\rho)}{F(n,1/2,n+5/2;\rho)}, \quad \text{(A7)}$$

$$c_n^V(\xi)=b_n^V(\xi)-\frac{4n(n+1)}{3(2n+5)(1+\xi)^2}$$
$$\times\frac{F(n+2,3/2,n+7/2;\rho)}{F(n,1/2,n+5/2;\rho)}. \quad \text{(A8)}$$

In Eqs. (A1) and (A5), m is the running quark mass $m=m_c[p^2=-(\xi+1)m_c^2]$, which is given by [56]

$$\frac{m_c(\xi)}{m_c(\xi=0)}=1-\frac{\alpha_s}{\pi}\left[\frac{2+\xi}{1+\xi}\ln(2+\xi)-2\ln 2\right]. \quad \text{(A9)}$$

[1] I. Arsene *et al.* (BRAHMS Collaboration), Nucl. Phys. **A757**, 1 (2005).
[2] B. B. Back *et al.* (PHOBOS Collaboration), Nucl. Phys. **A757**, 28 (2005).
[3] J. Adams *et al.* (STAR Collaboration), Nucl. Phys. **A757**, 102 (2005).
[4] K. Adcox *et al.* (PHENIX Collaboration), Nucl. Phys. **A757**, 184 (2005).
[5] M. Gyulassy and L. McLerran, Nucl. Phys. **A750**, 30 (2005).
[6] T. Matsui and H. Satz, Phys. Lett. **B178**, 416 (1986).
[7] S. S. Adler *et al.* (PHENIX Collaboration), Phys. Rev. C **69**, 014901 (2004).
[8] A. Adare *et al.* (PHENIX Collaboration), Phys. Rev. Lett. **98**, 232301 (2007).
[9] D. E. Kharzeev, J. Phys. G: Nucl. Part. Phys. **34**, S445 (2007).
[10] A. Andronic, P. Braun-Munzinger, K. Redlich, and J. Stachel, Phys. Lett. **B652**, 259 (2007).
[11] T. Umeda, R. Katayama, O. Miyamura, and H. Matsufuru, Int. J. Mod. Phys. A **16**, 2215 (2001).
[12] M. Asakawa and T. Hatsuda, Phys. Rev. Lett. **92**, 012001 (2004).
[13] S. Datta, F. Karsch, P. Petreczky, and I. Wetzorke, Phys. Rev. D **69**, 094507 (2004).
[14] T. H. Hansson, S. H. Lee, and I. Zahed, Phys. Rev. D **37**, 2672 (1988).
[15] S. J. Brodsky, I. Schmidt, and G. F. de Téramond, Phys. Rev. Lett. **64**, 1011 (1990).
[16] M. A. Shifman, A. I. Vainshtein, and V. I. Zakharov, Nucl. Phys. **B147**, 385 (1979).
[17] M. A. Shifman, A. I. Vainshtein, and V. I. Zakharov, Nucl. Phys. **B147**, 448 (1979).
[18] J. P. Blaizot, J. Phys. G: Nucl. Part. Phys. **34**, S243 (2007).
[19] L. J. Reinders, H. R. Rubinstein, and S. Yazaki, Nucl. Phys. **B186**, 109 (1981).
[20] R. J. Furnstahl, T. Hatsuda, and S. H. Lee, Phys. Rev. D **42**, 1744 (1990).
[21] F. Klingl, S. Kim, S. H. Lee, P. Morath, and W. Weise, Phys. Rev. Lett. **82**, 3396 (1999).
[22] A. Hayashigaki, Prog. Theor. Phys. **101**, 923 (1999).
[23] K. Morita and S. H. Lee, Phys. Rev. Lett. **100**, 022301 (2008).
[24] K. G. Wilson, Phys. Rev. **179**, 1499 (1969).
[25] S. C. Generalis and D. J. Broadhurst, Phys. Lett. **B139**, 85 (1984).
[26] E. M. Lifshitz and L. P. Pitaevskii, *Statistical Physics*, Part 2, Vol. 9 of *Course of Theoretical Physics* (Butterworth-Heinemann, Oxford, UK, 1980).
[27] T. Hatsuda, Y. Koike, and S. H. Lee, Nucl. Phys. **B394**, 221 (1993).
[28] A. I. Bochekarev and M. E. Shaposhnikov, Nucl. Phys. **B268**, 220 (1986).
[29] O. Kaczmarek, F. Karsch, F. Zantow, and P. Petreczky, Phys. Rev. D **70**, 074505 (2004).
[30] A. D. Giacomo and G. C. Rossi, Phys. Lett. **B100**, 481 (1981).
[31] A. D. Giacomo and G. Paffuti, Phys. Lett. **B108**, 327 (1982).
[32] M. Campostrini and A. D. Giacomo, Phys. Lett. **B197**, 403 (1987).
[33] S. H. Lee, Phys. Rev. D **40**, 2484 (1989).
[34] D. E. Miller, Phys. Rep. **443**, 55 (2007).
[35] G. Boyd, J. Engles, F. Karsch, E. Laermann, C. Legeland, M. Lütgemeier, and B. Petersson, Nucl. Phys. **B469**, 419 (1996).

[36] T. D. Cohen, R. J. Furnstahl, and D. K. Griegel, Phys. Rev. C **45**, 1881 (1992).
[37] B. Borasoy and U. G. Meißnner, Phys. Lett. **B365**, 285 (1996) .
[38] S. Leupold, W. Peters, and U. Mosel, Nucl. Phys. **A628**, 311 (1998).
[39] W. H. Press, S. A. Teukolsky, W. T. Vettering, and B. P. Flannery, *Numerical Recipes in Fortran 90* (Cambridge University Press, Cambridge, UK, 1996), Chap. 7.
[40] S. H. Lee and K. Morita, arXiv:0802.4000[hep-ph].
[41] Y. Park, K. I. Kim, T. Song, S. H. Lee, and C. Y. Wong, Phys. Rev. C **76**, 044907 (2007).
[42] S. H. Lee, Y. Park, K. I. Kim, and T. Song, J. Phys. G: Nucl. Part. Phys. **34**, S843 (2007).
[43] Y. Kim, J. P. Lee, and S. H. Lee, Phys. Rev. D **75**, 114008 (2007).
[44] F. Karsch and E. Laermann, in *Quark-Gluon Plasma 3*, edited by R. C. Hwa and X. N. Wang (World Scientific, Singapore, 2004), p. 1.
[45] C. Y. Wong, Phys. Rev. C **72**, 034906 (2005).
[46] G. Aarts, C. Allton, M. B. Oktay, M. Peardon, and J.-I. Skullerud, Phys. Rev. D **76**, 094513 (2007).
[47] T. Gunji, H. Hamagaki, T. Hatsuda, and T. Hirano, Phys. Rev. C **76**, 051901(R) (2007).
[48] K. Morita, Braz. J. Phys. **37**, 1039 (2007).
[49] B. Alessandro *et al.* (ALICE Collaboration), J. Phys. G: Nucl. Part. Phys. **32**, 1295 (2006).
[50] A. Andronic, P. Braun-Munzinger, K. Redlich, and J. Stachel, Nucl. Phys. **A789**, 334 (2007).
[51] S. H. Lee, AIP Conf. Proc. **717**, 780 (2004).
[52] C. A. Dominguez, M. Loewe, and J. C. Rojas, J. High Energy Phys. 08 (2007) 040.
[53] M. Cheng, N. H. Christ, S. Datta, J. van der Heide, C. Jung, F. Karsch, O. Kaczmarek, E. Laermann, R. D. Mawhinney, C. Miao *et al*., Phys. Rev. D **77**, 014511 (2008).
[54] F. Karsch, D. Kharzeev, and H. Satz, Phys. Lett. **B637**, 75 (2006).
[55] S. Kim and S. H. Lee, Nucl. Phys. **A679**, 517 (2001).
[56] V. A. Novikov, L. B. Okun, M. A. Shifman, A. I. Vainstein, M. B. Voloshin, and Z. I. Zakharov, Phys. Rep. **41**, 1 (1978).